PlanetMag: Software for evaluation of outer planet magnetic fields and corresponding excitations at their moons

Marshall J Styczinski[1] and Corey Jonathan Cochrane[2]

[1]Blue Marble Space Institute of Science
[2]Jet Propulsion Laboratory

April 12, 2024

PlanetMag: Software for evaluation of outer planet magnetic fields and corresponding excitations at their moons

M. J. Styczinski[1] and C. J. Cochrane[2]

[1]Blue Marble Space Institute of Science, Seattle, Washington, USA
[2]Jet Propulsion Laboratory, California Institute of Technology, Pasadena, California, USA

Key Points:

- We developed an open-source software package in Matlab called PlanetMag for evaluating planet magnetic field models from the literature
- PlanetMag uses ephemeris data and least-squares inversion methods to determine amplitudes and phases of magnetic excitations for moons
- Complex excitation moments are determined for all outer planet large moons in support of magnetic sounding investigations

Corresponding author: Marshall J. Styczinski, marshall.styczinski@bmsis.org

Abstract

Spacecraft magnetic field measurements are able to tell us much about the planets' interior dynamics, composition, and evolutionary timeline. Magnetic fields also serve as the source for passive magnetic sounding of moons. Time-varying magnetic fields experienced by the moons, due to relative planetary motion, interact electrically with conductive layers within these bodies (including salty subsurface oceans) to produce induced magnetic fields that are measurable by nearby, magnetometer-equipped spacecraft. Many factors influence the character of the induced field, including the precise amplitude and phase of the time-varying field, known as the excitation or driving field and represented by excitation moments. In this work, we present an open-source Matlab software package named PlanetMag that features calculation of planetary magnetic field models available in the literature at arbitrary positions and times. The implemented models enable simultaneous inversion of the excitation moments across a range of oscillation frequencies using linear least-squares methods and ephemeris data with the SPICE toolkit. Here we summarize the available magnetic field models and their associated coordinate systems. Precisely-determined excitation moments are a critical input to forward models of global induced fields. Our results serve as a prerequisite to any precise comparison to spacecraft data for magnetic sounding investigation of giant planet moons—connecting the induced magnetic field to a moon's interior requires accurate representation of the oscillating excitation field. We calculate complex excitation moments relative to the J2000 epoch and share the results as ASCII tables compatible with related software packages intended for induction response calculations.

Plain Language Summary

Planetary magnetic fields tell us much about a planet's interior, composition, and history. Magnetic fields are also useful for remotely probing the interior of their moons, especially for finding and characterizing potential subsurface oceans. Liquid-water oceans within the solar system are ideal places to search for habitable environments beyond Earth. Relating spacecraft magnetic measurements to the interior properties of the moons requires an understanding of various related components, including the manner in which the magnetic field applied to the moon changes with time. We have developed an open-source software package called *PlanetMag* that uses published magnetic field models to estimate the magnetic field at any point in time and space. It also has the ability to precisely estimate the planetary field oscillations at the location of each large moon in the solar system, which is needed for prediction of the magnetic field response from the moon. Calculations of these magnetic oscillations are provided in text files compatible with existing software.

1 Introduction

The giant planets—Jupiter, Saturn, Uranus, and Neptune—all have strong, internally generated magnetic fields (Schubert & Soderlund, 2011). The intrinsic field of each rotates with the planet. For this reason, they are believed to be generated deep in the interior, by the action of a *dynamo* (Stanley & Glatzmaier, 2010)—fluid motion of electrically conductive materials in the rotating frame of the planet generate stable magnetic fields. The magnetic fields of the planets demonstrate considerable variability. Properties of the dynamo region are expected to be what dictates the structure of the intrinsic field, which is represented by multipole magnetic moments. Multipole moments are spherical harmonic coefficients used to describe the magnetic field outside the body.

In the reference frame of each moon orbiting these planets, the ambient magnetic field oscillates with time, owing to non-zero eccentricity and inclination, the rotation of the parent planet to which the magnetic moments are fixed, or both. These relative planetary motions typically give rise to magnetic field variations at the orbital period of the moon and apparent rotation rate of the planet, respectively, due to positional differences between the two bodies. Time-varying magnetic fields drive electrical currents within conductive layers of the moons, thereby producing an induced magnetic field that is measurable outside the body.

Induced magnetic fields, properly isolated from other magnetic field contributions such as the background planetary field, fields associated with magnetospheric plasma currents, and spacecraft contaminate fields, can be used to detect and characterize subsurface saltwater and magma oceans. Magnetic measurements can thus be used to constrain the properties of subsurface oceans that affect the conductivity profile vs. depth, such as the thickness of ice crust and ocean layers, salinity and temperature profiles, etc. Indeed, such measurements have offered the strongest evidence yet available for the presence of a subsurface ocean within Europa (Kivelson et al., 2000), and have been used to place some constraints on the properties of its ocean and ice shell (Zimmer et al., 2000; Hand & Chyba, 2007; Schilling et al., 2007).

Magnetic sounding investigation of moons is a multi-step process. Relating magnetic measurements from a spacecraft to constraints on interior structure requires all of the following steps:

1. An estimate of the periodic oscillations in the applied field (the "excitation" field) in the frame of the moon
2. Hypothesized electrical conductivity structure of the interior—the layer configuration and conductivity of each
3. A calculation of the induced magnetic field consistent with both (1) and (2)
4. Removal of the planetary magnetic field, transient fields from plasma currents, and spacecraft fields from measurements
5. Statistical comparison of the induced magnetic field for each hypothesized interior structure (3) against measurements processed for background removal (4).

This work focuses primarily on the first of these steps.

The time-varying excitation field is best represented using complex coefficients that represent the amplitude and phase of the magnetic field vector components at the moon, called the excitation moments $\mathbf{B}^e$ (Styczinski et al., 2022). Excitation moments can be retrieved from a magnetic field time series derived from a planetary field model evaluated at the position of the moon. Spectral analysis (e.g., a Fourier transform) can be used to determine the specific frequencies or periods of the oscillations, while conventional linear least-squares (LLS) methods are able to estimate the amplitude and phases of the oscillations at different periods. There are numerous magnetic field models that are available in the literature, each developed by fitting a set of spherical harmonic coefficients to magnetometer data acquired by various spacecraft. Past studies examining Europa and Callisto (Kivelson et al., 1999) and Ganymede (Kivelson et al., 2002) have used simplified approximations of the excitation moments, typically considering only a single vector component with the largest amplitude (usually associated with the synodic period, the planet's apparent rotation rate in the frame of the moon). Past study of induction at Io (Khurana et al., 2011) included full vectors and additional excitation periods, but the authors did not provide sufficient information to determine how the relative phases of each component and period were handled or which magnetic field model was applied.

The spectra of magnetic oscillations experienced by the moons of the giant planets have been considered in past work. However, no prior studies have provided numerical results for both the amplitude and phase of the complex excitation moments that are required to calculate the induced magnetic field. Cochrane et al. (2021) and Cochrane et al. (2022) each performed a frequency decomposition of the excitation spectra for the moons of Uranus and Neptune, respectively, using an LLS inversion (see Section 2.1) in body-fixed frames defined by the International Astronomical Union (IAU), as in this work. Arridge and Eggington (2021) used a similar LLS inversion in study of the uranian moons. Biersteker et al. (2023) used an LLS inversion for Europa in the IAU frame as a test case, but the excitation moments were not detailed. All other prior studies have evaluated the amplitude of periodic oscillations using a Fast Fourier Transform (FFT) method, which is incapable of accurately determining the amplitudes and phases of excitation moments due to spectral leakage that results when one or multiple sinusoids are not perfectly periodic within the FFT sampling time series. The excitation spectra of Jupiter's large moons were evaluated in System III (1965) coordinates of the planet by Seufert et al. (2011) and in IAU frames by Vance et al. (2021, excluding Io). Excitation spectra for the large moons of Uranus were evaluated in System III coordinates by Arridge and Eggington (2021) and in moon-centric frames close to, but not identical to, IAU frames by Weiss et al. (2021). A detailed description of each coordinate system is contained in the supplemental material (Section S1).

In this work, we provide a means of calculating the complex excitation moments for all major moons of the giant planets relative to the J2000 epoch via the open-source framework *PlanetMag* and include ASCII tables of results for each moon (Styczinski & Cochrane, 2024c). Magnetic field models for the internal and external contributions (e.g., current sheets, magnetopause currents, etc.) are available in the literature, but the diversity of employed coordinate systems, model formats, and software inconsistencies can make evaluation of these models difficult and time consuming. Software for evaluation of some models is available, but existing frameworks are limited in scope (Table 1). *PlanetMag* includes all peer-reviewed magnetospheric field models for all of the giant planets in a common Matlab package, which can be evaluated at arbitrary locations and times. Each model is validated against magnetic measurements from relevant spacecraft available from the Planetary Data System (PDS, see Table 4). Spacecraft, planet, and moon positions and trajectories are precisely determined for any input time by integration with the SPICE toolkit developed by the NASA Navigation and Ancillary Information Facility (NAIF; Acton, 1996). The excitation moments are evaluated for each moon for a selected model over an era relevant to a selected spacecraft. A limited duration pertaining to the residence time of a spacecraft must be selected because the orbital and rotational parameters of the planets and moons drift over time due to tidal forcing, and so too must the excitation moments.

Our prior work has used excitation moments calculated from precursors to what has now become *PlanetMag*: Vance et al. (2021); Styczinski et al. (2021); Cochrane et al. (2021); Styczinski et al. (2022); Cochrane et al. (2022); Biersteker et al. (2023); Plattner et al. (2023). Because of the variation in magnetic field that is expected over long time periods (known as secular variation), for future missions that entail multiple moon flybys such as Europa Clipper (Vance et al., 2023) and JUICE (Fletcher et al., 2023), the excitation moments can be more accurately solved for directly from joint flyby measurements. However, for single-flyby mission concepts, where long periods cannot be measured over the course of the mission, using excitation moments extracted from a magnetic field model as described in this work is essential for magnetic investigation of icy bodies (Cochrane et al., 2022).

Several open-source software libraries and frameworks are already available for the evaluation of planetary field models for the outer planets, detailed in Table 1. Most available models focus on a single planet. To our knowledge, Table 1 includes all currently available open-source software packages for evaluation of giant planet magnetic fields as of this writing. No available models include features for calculation of excitation moments or integration with SPICE. Therefore, we created *PlanetMag* (Styczinski & Cochrane, 2024b) to offer these features within a single software package. The software is thoroughly documented (documentation is available at `https://coreyjcochrane.github.io/PlanetMag/`) and a Python port is in development.

Table 1. Open-source software packages currently available for evaluation of planetary magnetic field models. All packages focus on a single planet except *planetMagFields* and *libinternalfield*, both of which feature only intrinsic field models. None of the available packages features a calculation of excitation moments or integration with SPICE, both of which we implement in *PlanetMag*.

Package name	Planet	Language(s)	Archive reference	Publication
KS2005	Jupiter	IDL	N/A[a]	Khurana and Schwarzl (2005)
KMAG2012	Saturn	Fortran	Khurana (2020)[b]	N/A
JupiterMag[c]	Jupiter	Python and C++[d]	James et al. (2024a)[e]	Wilson et al. (2023)
PSH	Jupiter	Python, Matlab, IDL	Wilson et al. (2022)[f]	Wilson et al. (2023)
Saturn-Mag-Model	Saturn	Python, Matlab, IDL	N/A[g]	N/A
planetMagFields	All planets	Python	Barik and Angappan (2024a)[h]	Barik and Angappan (2024b)
libinternalfield	All planets	Python and C++[d]	N/A[i]	N/A

[a]Non-archived IDL code is currently available at `https://lasp.colorado.edu/mop/resources/code/`.

[b]A Python wrapper for running the Fortran code (requiring both Python and Fortran) is also available (Rusaitis, 2022).

[c]Relies on a C++ module, *libjupitermag* (James et al., 2024b): `https://github.com/mattkjames7/libjupitermag`

[d]Both Python and C++ are required.

Available GitHub repositories:

[e]`https://github.com/mattkjames7/JupiterMag`

[f]`https://github.com/rjwilson-LASP/PSH`

[g]`https://github.com/NASA-Planetary-Science/Saturn-Mag-Model`

[h]`https://github.com/AnkitBarik/planetMagFields`

[i]`https://github.com/mattkjames7/libinternalfield`

2 Methods

For most moons, the magnetic field of the parent planet varies little on the spatial scale of the moon. As a result, it is customary to consider only the oscillations in the mean field across each moon, approximated as that evaluated at the body center. Notable exceptions are Io, with as much as a 58 nT difference, Europa with a 7.3 nT difference, and Mimas with a 4.9 nT difference from the sub-planetary point to its antipode, all of which we have calculated using the default models implemented in *PlanetMag* (Tables 2 and 3). Periodic oscillations in the difference in the local magnetic field across the body contribute excitation moments of degree 2 and higher, which will decay faster than $1/r^3$ except in the case of highly asymmetric bodies (Styczinski et al., 2022). Magnetic induction from excitations of degree 2 may be significant for sounding of Io, but calculation of these moments is left for future work.

Excitation moments associated with the time-varying portion of the mean field are of spherical harmonic degree 1 and can be represented by complex vector components aligned to the axes of the desired coordinate system. The ambient field at the body center at time t can be represented with

$$\mathbf{B}_{\mathrm{amb}}(t) = \sum_k \mathbf{B}_k^e e^{-\mathrm{i}\omega_k t}, \tag{1}$$

where $\mathbf{B}_k^e$ are the time-varying field vectors periodically oscillating at angular frequencies ω_k, including the static field at $\omega_{\mathrm{DC}} = 0$. The ambient field is complex in general—the measurable field is evaluated by taking the real part of the complex total (Jackson, 1999).

To retrieve the excitation moments in the frame of the moon, we first determine the location of the moon in the coordinates of the planetary field model using SPICE—each required frame is defined in our custom frames kernel or built-in to the SPICE satellites kernels. Next, we evaluate the planetary magnetic field model (Tables 2 and 3) over a period of time that spans the desired epoch with a number of sampling times N (by default, $\mathcal{O}(10^6)$) and rotate this field vector into the desired frame of the moon using transformation functions implemented in SPICE. The excitation moments can then be extracted from the resultant time series, $\mathbf{B}_i = \mathbf{B}_{\mathrm{model}}(t_i)$. For rapid evaluation of the underlying models in *PlanetMag*, we have implemented a direct calculation of spherical harmonics and their derivatives in the Schmidt normalization up to degree 10. At distances of the orbiting moons, the higher-degree harmonics have negligible contributions. We have

Table 2. Model combinations implemented in *PlanetMag* for Jupiter. The default model, under which we have calculated excitation moments for the major moons, is highlighted in **bold.** Parameters for each model are hard-coded, with spherical harmonic coefficients read from text files at run time. Analytical current sheet models for both C1981 and C2020 use the formulation of Connerney et al. (1981) with overall fit parameters listed in each publication.

Model name	Description and references
VIP4+C1981	Voyager–Io flux tube footprint–Pioneer degree-4 model of Connerney et al. (1998) (more precisely reported by Connerney (2007)) along with the analytical current sheet model of Connerney et al. (1981).
O6+K	Degree-6 partial fit of Connerney (1992) to primarily Voyager 1 magnetic data, along with the current sheet model of Khurana (1997).
KS2005	Combined magnetosphere model of Khurana and Schwarzl (2005). Uses the VIP4 intrinsic field model, but with the dipole moment rotated to match the O6 orientation, and a current sheet model constrained by crossings inferred from magnetic data of Galileo and all prior spacecraft to visit the planet.
JRM09+C2020	Juno Reference Model through 9 orbits, a degree-20 intrinsic field model (Connerney et al., 2018) and the analytical current sheet model of Connerney et al. (2020), updated to pair with the JRM09 model. Both are fit to Juno data. Moments are well-resolved up to degree 10. For C2020, we use the overall fit parameters contained in Table 1 of Connerney et al. (2020).
JRM09+C1981	JRM09 model with current sheet of Connerney et al. (1981). This is the model used by Vance et al. (2021).
VIP4+K	VIP4 model with current sheet of (Khurana, 1997). This is the model studied by Seufert et al. (2011).
JRM33+C2020	Degree-30 intrinsic field of Connerney et al. (2022) through Juno's first 33 orbits along with current sheet model of Connerney et al. (2020), also fit to Juno data. Moments up to degree 13 are well-resolved.

Table 3. Models implemented in *PlanetMag* for planets beyond Jupiter. Default models, under which we have calculated excitation moments for the major moons, are highlighted in **bold.** Parameters for each model are hard-coded, with spherical harmonic coefficients read from text files at run time. Analytical current sheet models for Cassini 11 use the formulation of Connerney et al. (1981) with overall fit parameters listed in Dougherty et al. (2018).

Model name	Planet	Description and references
B2010	Saturn	Intrinsic field model of Burton et al. (2010) fit to Cassini magnetic data. Includes a degree-1 fit to an externally applied field.
Cassini 11	Saturn	Degree-12 (with only up to degree 11 well-resolved) intrinsic field model of Dougherty et al. (2018) fit to Cassini magnetic data, including from the Grand Finale orbits. Includes a current sheet model.
Cassini 11+	**Saturn**	Degree-14 intrinsic field model of Cao et al. (2020); similar to Cassini 11 but with different regularization and using a subset of Grand Finale orbits.
Q3	Uranus	Quadrupole-resolved, degree-3 fit of Connerney (1987) to Voyager 2 magnetic data. Includes a degree-1 fit to an externally applied field.
AH5	**Uranus**	Auroral Hexadecapole $L = 5$ intrinsic field model of Herbert (2009). Moments up to degree 4 fit to Voyager 2 magnetic data and auroral observations. This is the model studied by Weiss et al. (2021) and Cochrane et al. (2021)[a].
O8	**Neptune**	Degree-8 intrinsic field model of Connerney et al. (1992) fit to Voyager 2 magnetic data. Moments above degree 3 are not uniquely determined.

[a] Also studied by Arridge and Eggington (2021) along with a magnetopause model.

also have begun to implement an evaluation of each available model of the magnetic fields from selected magnetopause current models, but these models are considered preliminary and have not been used in determining the excitation moments in this work.

Numerous coordinate systems have been considered in past magnetic sounding investigations. In this work, we evaluate all excitation moments in the IAU frame of each moon in Cartesian coordinates. This approach has several advantages. The IAU frames are implemented in all SPICE kernels containing the moons, which enables simple conversion between coordinate systems and evaluation of spacecraft trajectories using functions built-in to SPICE. More importantly, IAU frames are fixed to the surface of the body. Integration with SPICE in evaluating the excitation moments in the frame of the body thus enables a proper accounting for all motional effects on the periodic components of the excitation field, including libration, apsidal precession, etc. These effects are significant for some bodies, as in the case of Europa, where excitation at the true anomaly period (TA; the time between periapsis crossings) differs from that at the orbital period (the time between ascending node crossings), including in terms of the affected components (Table 5). IAU frames are the only ones considered in past work that have been body-fixed frames. See Section S1 for a description of the IAU frames and others implemented in *PlanetMag*, including those used in past studies.

2.1 Inversion of excitation moments

Using the magnetic field vector time series $\mathbf{B}_i$ sampled at times t_i in the IAU frame of a moon, we perform a frequency decomposition of the excitation moments using an LLS optimization approach. The model magnetic field can be estimated as the real part of a superposition of sinusoids in terms of the excitation moments and their corresponding angular frequencies:

$$\mathbf{B}_{\mathrm{model}}(t) \approx \mathrm{Re}\{\mathbf{B}_{\mathrm{amb}}(t)\} = \sum_k \left[\mathbf{B}^e_{k,\mathrm{Re}} \cos(\omega_k t) + \mathbf{B}^e_{k,\mathrm{Im}} \sin(\omega_k t)\right], \quad (2)$$

where $\mathbf{B}^e_k = \mathbf{B}^e_{k,\mathrm{Re}} + \mathrm{i}\mathbf{B}^e_{k,\mathrm{Im}}$. These coefficients can be found by minimizing the sum of squared errors, i.e. $\sum_i(\mathbf{B}_{\mathrm{model}}(t_i) - \mathrm{Re}\{\mathbf{B}_{\mathrm{amb}}(t_i)\})^2$. There are a total of $6F+3$ coefficients for each inversion, where F is the number of frequencies used in the inversion. This includes 6 coefficients for every excitation frequency—the real and imaginary part for each vector component of the magnetic field vector—and 3 coefficients in the static background magnetic field vector.

In the following, the index k refers specifically to the real or imaginary part of a frequency component. Given a list of expected excitation frequencies $\mathbf{f} = \{f_k\}$, the LLS-optimized coefficients for the excitation moments can be directly calculated using classical methods (for reference, see Markovsky & Van Huffel, 2007). The LLS inversion is calculated as follows. For $\omega_k = 2\pi f_k$, the columns of the design matrix X_{ik} are $\cos(\omega_k t_i)$ for the real part of each excitation moment and $\sin(\omega_k t_i)$ for the imaginary part. Each row in X_{ik} corresponds to a time t_i in the time series, i.e.

$$X_{ik} = \begin{bmatrix} \cos(\omega_1 t_1) & \sin(\omega_1 t_1) & \cos(\omega_2 t_1) & \sin(\omega_2 t_1) & \dots & \cos(\omega_F t_1) & \sin(\omega_F t_1) & 1 \\ \cos(\omega_1 t_2) & \sin(\omega_1 t_2) & \cos(\omega_2 t_2) & \sin(\omega_2 t_2) & \dots & \cos(\omega_F t_2) & \sin(\omega_F t_2) & 1 \\ \vdots & \vdots & \vdots & \vdots & \ddots & \vdots & \vdots & \vdots \\ \cos(\omega_1 t_N) & \sin(\omega_1 t_N) & \cos(\omega_2 t_N) & \sin(\omega_2 t_N) & \dots & \cos(\omega_F t_N) & \sin(\omega_F t_N) & 1 \end{bmatrix}. \tag{3}$$

The same design matrix with $2F+1$ columns is used for each vector component. The eigenvectors of X_{ik} are the columns of the weight matrix W, such that

$$W = \left(X_{ik}^T X_{ik}\right)^{-1} \tag{4}$$

$$B^e_{j,k} = (\mathbf{B}_i \cdot \hat{\mathbf{e}}_j) X_{ik} W, \tag{5}$$

where $B^e_{j,k}$ lists the real and imaginary parts of the excitation moment for vector component j and $\hat{\mathbf{e}}_j$ is a unit vector in the direction of component j. The product $X_{ik}W$ is commonly referred to as the pseudo-inverse. The results for $B^e_{j,k}$ from Equation 5 are those that minimize the sum of squared errors. The complex excitation moments for each frequency k are then constructed from

$$\mathbf{B}^e_k = \sum_j \left(B^e_{j,k,\mathrm{Re}} + \mathrm{i} B^e_{j,k,\mathrm{Im}}\right) \hat{\mathbf{e}}_j \tag{6}$$

and the LLS fit to the input time series can be evaluated with

$$\mathbf{B}_{\mathrm{amb}} = (\mathbf{B}^e_k)^T X_{ik}. \tag{7}$$

The list of excitation frequencies $\mathbf{f}$ of the moments are identified from the natural spectrum of oscillations in an FFT of the time series $\mathbf{B}_i$. Each Fourier spectrum is rich in driving field oscillations, typically including the synodic period, the orbital period, and the harmonics and beats of these two fundamental periods. These frequencies are precisely calculated from information contained in cartographic reports (see Section S1.1 in the supplemental material) and retrieved from the SPICE planetary constants kernel.

The list $\mathbf{f}$ is refined iteratively in order to best reproduce the time series $\mathbf{B}_i$ with Equation 2 after inverting for the excitation moments. At each of the following steps, we evaluate an FFT of the residuals, i.e. the difference between the input time series and its reproduction using Equation 2. The process is continued until the residual spectrum has no peaks over 1 nT, a commonly considered detection threshold, and minimal peaks below this threshold, which essentially represent noise. An example residual FFT for the magnetic field that Europa experiences, after completion of this process, is shown in Figure 1.

We first find the excitation moments with just the known synodic period and sidereal orbit period. Next, we add a wide array of beats and harmonics associated with these excitation periods. The frequencies of remaining unknown peaks in the residual spectrum are determined numerically using linear combinations of the leakage-spread points in the spectrum near the peak, successively until the peak is precisely determined. Examples of such peaks unrelated to beats and harmonics include true anomaly periods for moons with marked apsidal precession, including Europa and Enceladus. After each such peak is precisely determined, its harmonics and beats with other excitation periods are added to $\mathbf{f}$. Finally, once all peaks in the residual spectrum are below 1 nT, frequencies are removed from $\mathbf{f}$, starting with those associated with the lowest amplitudes in the LLS-inverted excitation moments, until as few amplitudes below 1 nT are included among the moments and no peaks in the residual spectrum are over 1 nT.

2.2 Model validation

To confirm the correct implementation of the many models we have included in *PlanetMag*, we compare each against spacecraft magnetic measurements gathered near the relevant planet. The datasets we compare are all available from the PDS. All data comparisons demonstrate close agreement with the evaluated model (Figure 2).

PlanetMag employs a direct calculation of spherical harmonics and their derivatives up to degree 10 in spherical coordinates in the Schmidt normalization for evaluation of intrinsic field models. In order to confirm that these calculations have been implemented correctly, we undertook a cross-comparison with the same calculations under different normalizations with *MoonMag* (Styczinski, 2023). *MoonMag* features the same calculations with complex, orthonormal spherical harmonics and with real-valued

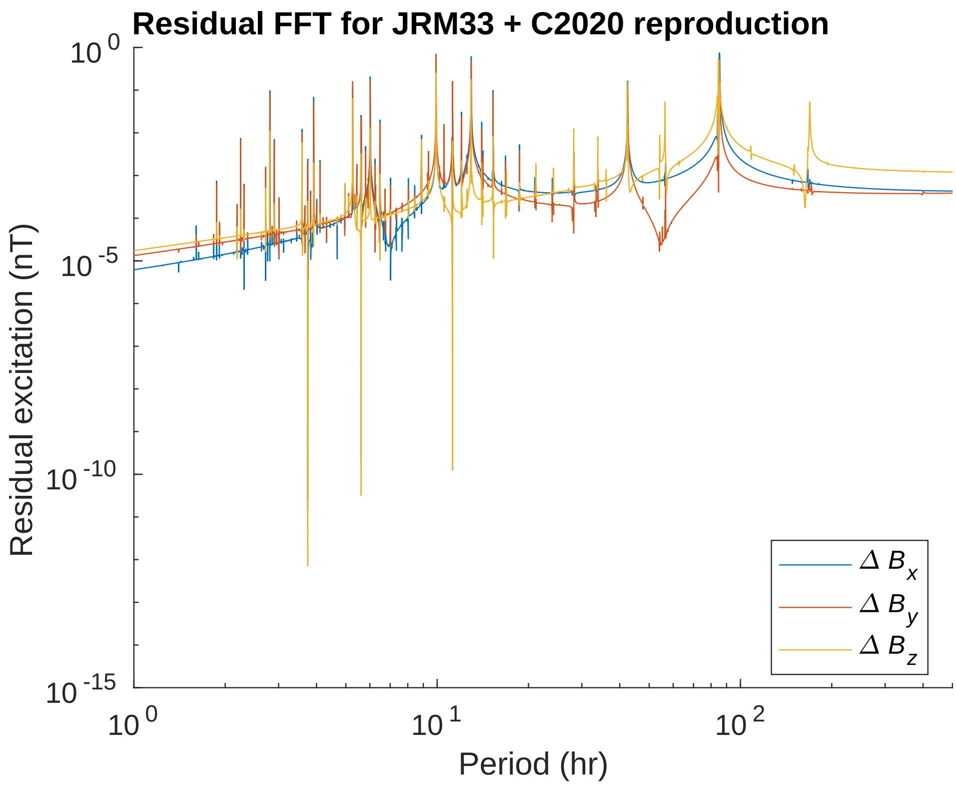

Figure 1. Fast Fourier Transform (FFT) of the residuals from inversion of the excitation spectrum for Europa, during the Juno era and with the JRM33+C2020 model as detailed in Table 2. The residuals are the differences for each evaluation time between a vector component of the model field and the reproduction generated with the inverted excitation moments, i.e. $\Delta\mathbf{B}_i = \mathbf{B}_{\mathrm{model}}(t_i) - \mathrm{Re}\{\mathbf{B}_{\mathrm{amb}}(t_i)\}$. Several key excitation periods that are very stable over the input era exhibit a marked reduction in power in the residual spectrum, demonstrating that these excitation periods are well-represented by the inverted moments. Some other excitations, such as those at the true anomaly and orbital periods, do not show the same reduction despite being well-captured because these periods drift over time.

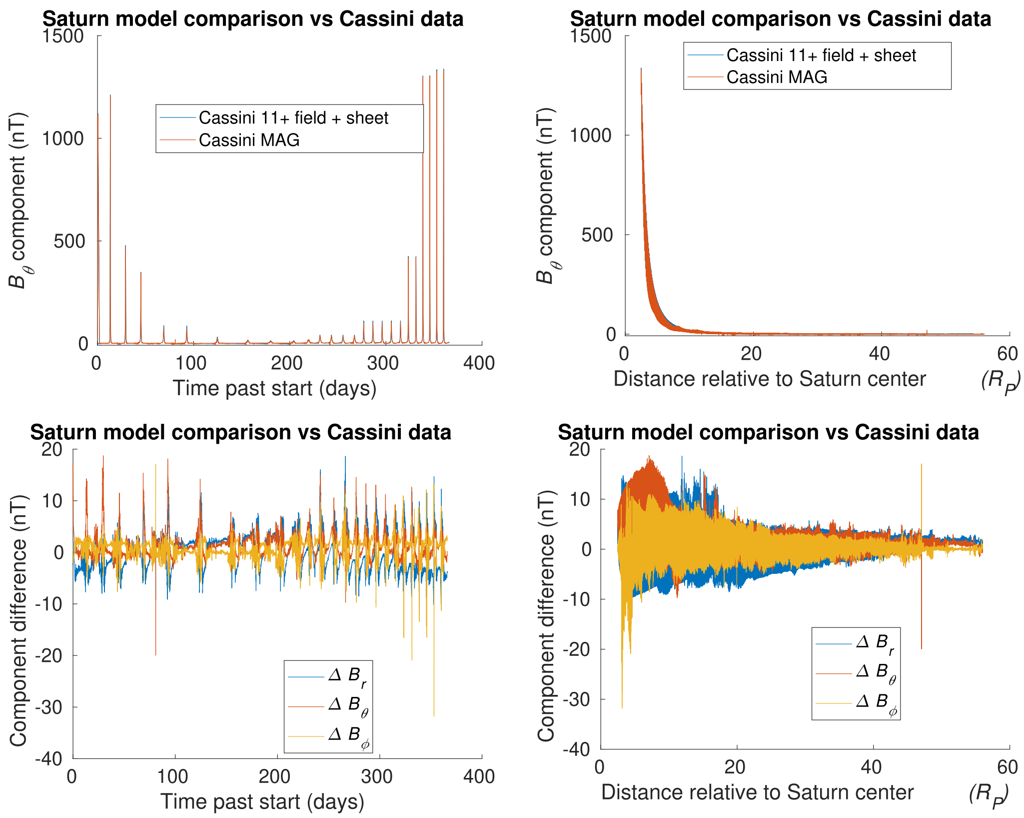

Figure 2. Comparison of Cassini 11+ model predictions and measurements from the Cassini spacecraft for the B_θ component (top) and differences for all components (bottom) in System III spherical coordinates during the year 2016. Each row shows the same data—on the left, the comparison is chronological, and on the right, the comparison is organized by distance from Saturn. Models implemented for the other giant planets show similar agreement with the compared measurements.

Table 4. Default combinations of planetary magnetic field models and data sources used for validation. Implemented models are described in Tables 2 and 3. In each case, we have used "survey" or "summary" data, which are averaged or decimated to provide lower-rate measurements that are more manageable for analyses over long time scales. We used Juno (1 s planetocentric) and high-resolution Galileo data only in validating model evaluation and calculation of the externally applied field from the excitation moments using Equation 7 against moon encounter data.

Planet	Default model	Spacecraft	PDS data volume
Jupiter	JRM33+C2020	Galileo, Juno	GO-J-MAG-3-RDR-MAGSPHERIC-SURVEY-V1.0 (Kivelson et al., 1997b), GO-J-MAG-3-RDR-HIGHRES-V1.0 (Kivelson et al., 1997a), JNO-J-3-FGM-CAL-V1.0 (Connerney, 2022)
Saturn	Cassini 11+	Cassini	CO-E/SW/J/S-MAG-4-SUMM-1MINAVG-V2.1 (Dougherty et al., 2019)
Uranus	AH5	Voyager 2	VG2-U-MAG-4-SUMM-U1COORDS-48SEC-V1.0 (Ness, 1993)
Neptune	O8	Voyager 2	VG2-N-MAG-4-SUMM-NLSCOORDS-12SEC-V1.0 (Ness, 1989)

Schmidt-normalized harmonics, both in Cartesian coordinates. We constructed a HEALpix map (Gorski et al., 2005) for evaluation under all 3 methods of calculating the magnetic field at the planet surface for each pure multipole moment (e.g., each combination of n, m, and $\sin m\phi$ or $\cos m\phi$) and compared the results, addressing any discrepancies until all methods produced the same results up to machine precision.

3 Results

The magnitude of the magnetic field for each of the giant planets evaluated with *PlanetMag* at the IAU-defined planetary radius is shown in Figure 3. *PlanetMag* is designed for evaluation of planetary field models at arbitrary locations and times in the middle magnetosphere for each planet, where the majority of the moons reside. Magnetodisk models and spherical-harmonic intrinsic field models break down at distances

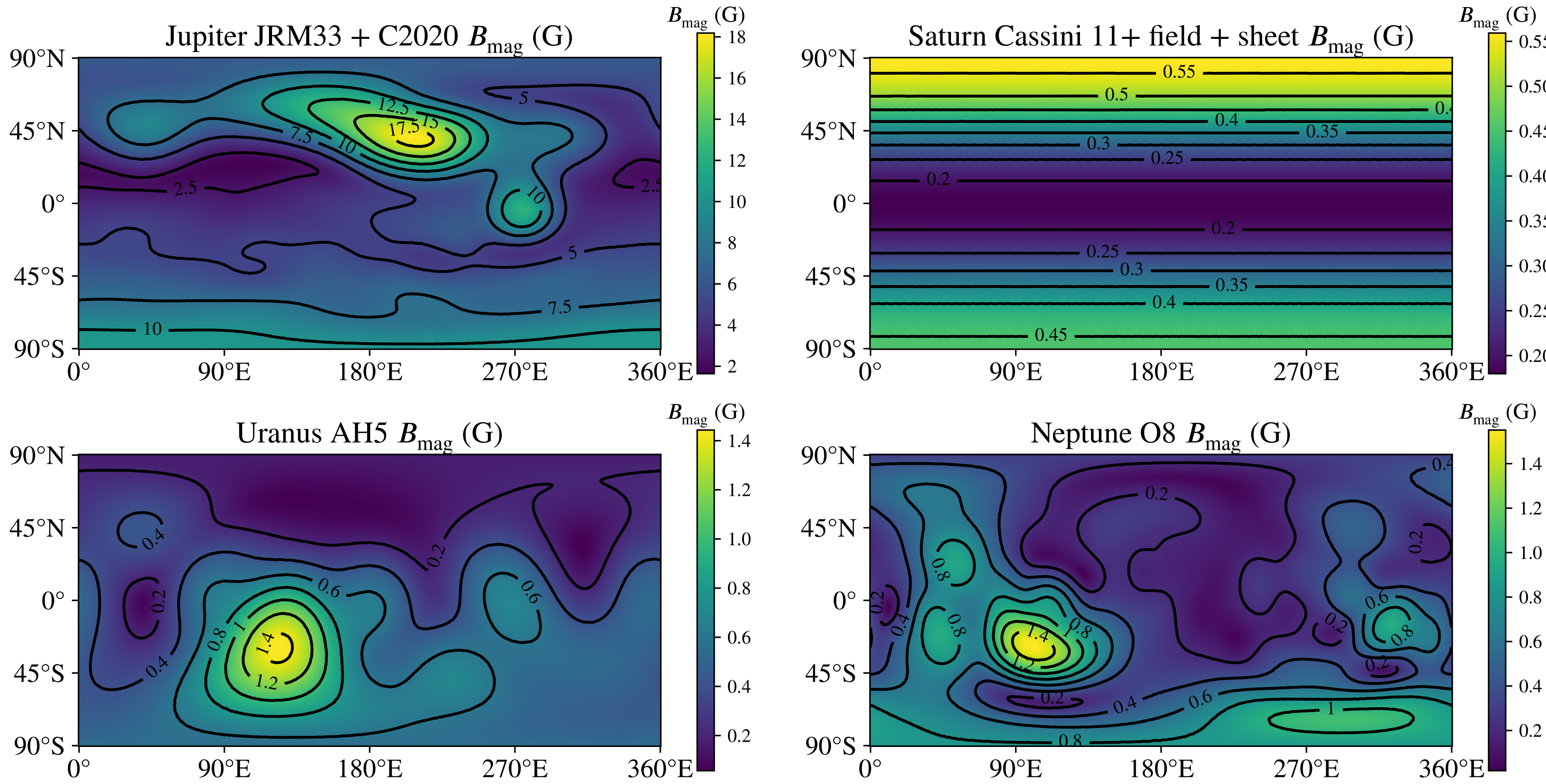

Figure 3. Magnetic field magnitude in gauss evaluated with *PlanetMag* at the IAU-defined equatorial radius for each planet, i.e. the 1 bar radius, in planetocentric System III coordinates. Jupiter: $R_J = 71492\,\text{km}$; Saturn: $R_S = 60268\,\text{km}$; Uranus: $R_U = 25559\,\text{km}$; Neptune: $R_N = 24764\,\text{km}$. Note that comparison to similar diagrams from past studies (e.g., Connerney et al., 2022) shows similar trends, but use of planetocentric vs. planetographic coordinates and our degree-10 limit for the intrinsic field will exhibit some differences on short distance scales.

on the scale of the magnetopause standoff distance (e.g., $\sim 50R_J$ for Jupiter) and limiting our evaluation to degree 10 for the intrinsic field means that regions within $1-2$ planetary radii of the 1 bar surface will not be modeled accurately due to the missing higher-order moments. We have used the capabilities of our implementation with the default models described in Tables 2 and 3, precise ephemerides from SPICE, and our LLS inversion method to determine the excitation moments for all major moons in the outer solar system. A subset of the excitation moments for Europa is detailed in Table 5. The excitation field can be calculated at arbitrary times using Equation 2. For example, ignoring the smaller excitations not included in Table 5, the instantaneous excitation field at Europa $\mathbf{B}_{\mathrm{amb}}(t)$ in the IAU frame is computed with

$$\begin{aligned}\mathbf{B}_{\mathrm{amb}}(t) \approx\, &\mathrm{Re}\{\mathbf{B}^e_{\mathrm{syn}}\}\cos(\omega_{\mathrm{syn}}t) + \mathrm{Im}\{\mathbf{B}^e_{\mathrm{syn}}\}\sin(\omega_{\mathrm{syn}}t) + \\ &\mathrm{Re}\{\mathbf{B}^e_{\mathrm{synHarm}}\}\cos(\omega_{\mathrm{synHarm}}t) + \mathrm{Im}\{\mathbf{B}^e_{\mathrm{synHarm}}\}\sin(\omega_{\mathrm{synHarm}}t) + \\ &\mathrm{Re}\{\mathbf{B}^e_{\mathrm{orb}}\}\cos(\omega_{\mathrm{orb}}t) + \mathrm{Im}\{\mathbf{B}^e_{\mathrm{orb}}\}\sin(\omega_{\mathrm{orb}}t) + \\ &\mathrm{Re}\{\mathbf{B}^e_{\mathrm{TA}}\}\cos(\omega_{\mathrm{TA}}t) + \mathrm{Im}\{\mathbf{B}^e_{\mathrm{TA}}\}\sin(\omega_{\mathrm{TA}}t) + \\ &\mathrm{Re}\{\mathbf{B}^e_{\mathrm{syn-TA}}\}\cos(\omega_{\mathrm{syn-TA}}t) + \mathrm{Im}\{\mathbf{B}^e_{\mathrm{syn-TA}}\}\sin(\omega_{\mathrm{syn-TA}}t),\end{aligned} \tag{8}$$

where t is in TDB seconds relative to J2000 (also called ephemeris time ET in SPICE), $\omega_k = 2\pi/T_k$ with T_k in s, and $\mathbf{B}^e_k$ are the complex excitation moment vectors listed in Table 5. The full set of excitation moments we have calculated using default models is compiled into ASCII data tables (Styczinski & Cochrane, 2024c).

Hodograms showing a planar projection of the path traced by the magnetic field vector in a selected plane are shown in Figure 4. Lines in these diagrams appear thick or smeared due to superposition of multiple excitations, each contributing vectors of varying amplitudes and phases. The hodograms have been constructed from the same data as those used to calculate the excitation moments—a time series of the default model for each planet at the location of each moon for approximately 10^6 equally-spaced time steps spanning a particular era. We chose the Juno era for Io, Europa, and Ganymede due to relevance for analyzing Juno flyby data from each moon, and the Galileo era for Callisto. We used the VIP4+K model to calculate the excitation moments for Callisto instead of the default in Table 2. This is because the planar models of Connerney et al. (1981) and Connerney et al. (2020) do not capture the bendback of the current sheet, which contributes significantly to the field at Callisto's relatively large orbital distance (about $26.3R_J$), as compared to hinged current sheet models such as Khurana (1997)

Table 5. Example excitation moments for the 5 strongest oscillations at Europa over the Juno era, relative to the J2000 epoch. These moments were evaluated with the JRM33 intrinsic field model (Connerney et al., 2022) and the analytical current sheet model of Connerney et al. (2020). No magnetopause currents were modeled in calculating these values. A full list of excitation moments for all large moons of the giant planets and for all implemented models and spacecraft eras is available as a Zenodo archive (Styczinski & Cochrane, 2024c).

Excitation name	Period (h)	Excitation moment vector (IAU frame, nT)
Synodic	11.23	$(131.4 - 173.1\mathrm{i})\hat{x} + (-65.5 - 35.4\mathrm{i})\hat{y} + (-4.8 - 15.2\mathrm{i})\hat{z}$
Synodic harmonic	5.62	$(16.8 + 4.7\mathrm{i})\hat{x} + (2.9 - 11.3\mathrm{i})\hat{y} + (1.3 + 1.6\mathrm{i})\hat{z}$
Orbital	85.2	$(-7.4 + 7.7\mathrm{i})\hat{x} + (-2.3 - 2.7\mathrm{i})\hat{y} + 0.5\mathrm{i}\hat{z}$
True anomaly (TA)	84.6	$(-0.5 - 0.1)\mathrm{i}\hat{x} - 0.2\hat{y} + (8.6 - 5.9\mathrm{i})\hat{z}$
Synodic−TA beat	12.95	$(4.6 + 2.3\mathrm{i})\hat{x} + (1.6 - 3.4\mathrm{i})\hat{y} + (0.4 - 0.2\mathrm{i})\hat{z}$

(Khurana & Schwarzl, 2005). For the moons of Saturn, we used the Cassini era because of the wealth of data available from that mission. For moons of Uranus and Neptune, we used the Voyager era, a 6-month period centered on the Voyager 2 flyby of each planet from which in situ data were gathered.

The excitation moments shift over time and will yield different results when calculated with different planetary field models. All magnetic field models implemented in *PlanetMag* can be used to calculate excitation moments over any duration supported by the loaded SPICE kernels.

4 Discussion and conclusions

The planetary magnetic field models in *PlanetMag* show favorable comparison to the spacecraft measurements from which the models were derived (e.g., Figure 2), which implies they have been correctly implemented. Spurious signals from disturbances in the surrounding plasma environment, which are not captured in planetary field models, will not affect the long-term periodicity of the excitation field, and so will not affect the excitation moments. However, periodic motion or variance in the plasma around each moon, oscillating at the same key periods, especially that driven by the same excitations as those we calculate in this work, will affect the excitation moments. Accounting for such effects

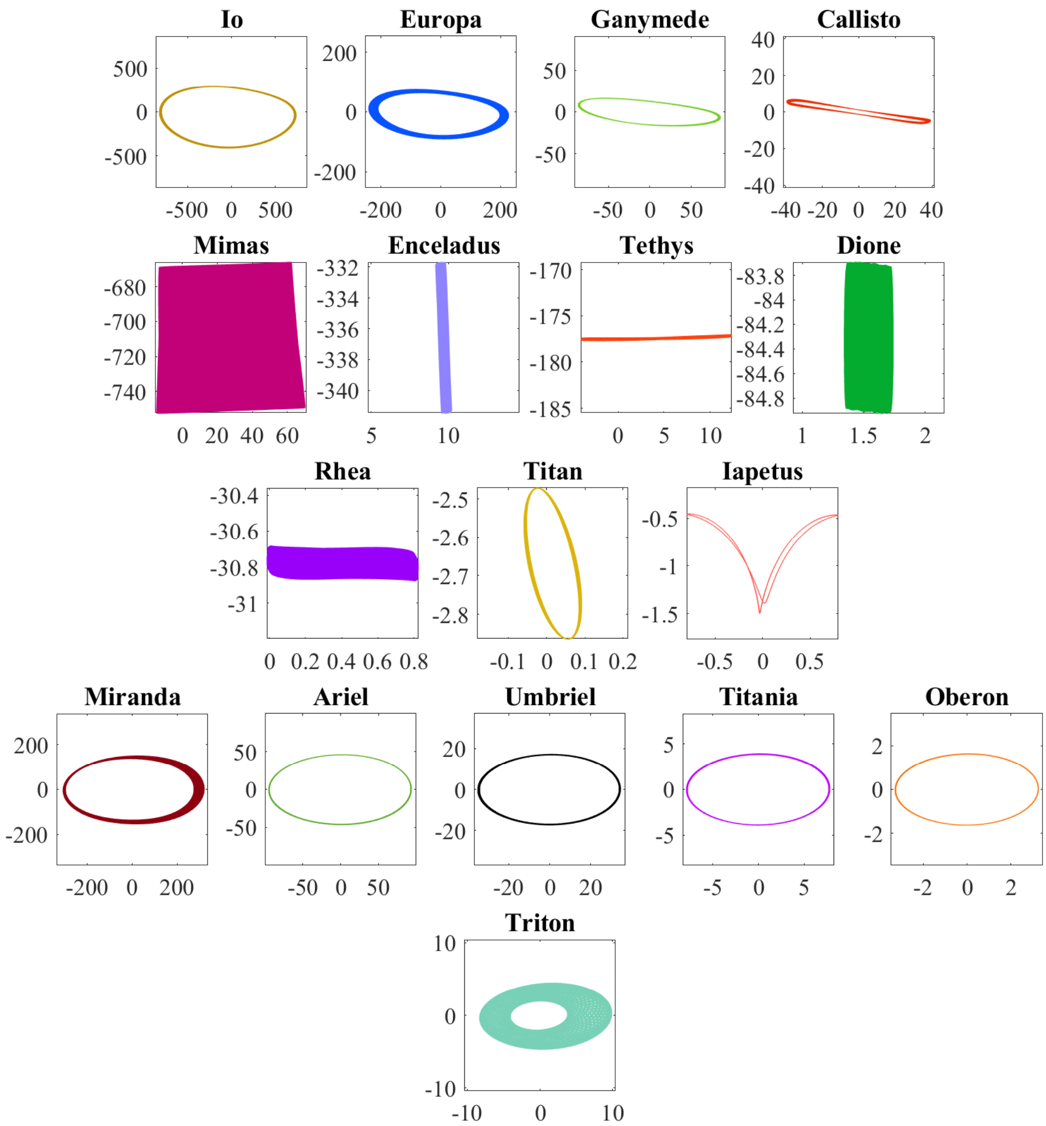

Figure 4. Hodograms for large moons in the outer solar system. The represented data are those used to calculate the excitation moments (Styczinski & Cochrane, 2024c), i.e. the default models in Tables 2 and 3, except for Callisto, for which we have used VIP4+K. Each diagram shows the path traced by the tip of the magnetic field vector projected into the IAU xy (equatorial) plane in nT, except for the moons of Saturn which show the IAU xz plane. All panels have an equal aspect ratio, showing an equivalent range along both axes.

is beyond the scope of this work. The principle of superposition dictates that the contributions from plasma can be summed independently from those of the excitation field from the broader magnetosphere, but the contributions from plasma that react to the same excitations will tend to decrease the driving field and thus change the net time-varying field in the frame of the moon.

The effects of periodic variance in the plasma environment have never been self-consistently modeled along with the excitation field in magnetic sounding investigations, although Schilling et al. (2007) modeled how the variance in Europa's plasma environment may affect inferences of its interior structure. Future work, including analysis of measurements from the Europa Clipper mission, must account for periodicity in the plasma environment to most accurately estimate the excitation moments applied to the moon. Plasma motion may also contribute its own excitations at periods not matching those from the planetary field (e.g., Schilling et al., 2008; Blöcker et al., 2016; Harris et al., 2021), which could confound efforts to isolate the induced magnetic field.

Magnetic fields in the frame of each moon are not constructed of perfectly sinusoidal contributions, so the excitation moments can never perfectly reproduce the input time series. The excitation frequencies $\mathbf{f}$ are not constant over time, because tidal perturbations from mutual gravity and the dissipation of energy inside each body change their orbital elements and rotational properties over time. Many such effects are considered in the development of IAU frames and in trajectory calculations with SPICE. However, while accounting for these drifts in motional parameters promotes a more complete description of excitation moments, as in the case of the TA period at Europa, it also adds a small amount of noise to the excitation spectrum. This is why the orbital and TA periods do not show the same dramatic reduction in represented power as the shorter-period, more stable excitations in the residual spectrum for Europa (Figure 1).

As currently implemented in *PlanetMag*, the list of excitation frequencies $\mathbf{f}$ used to define the design matrix X_{ik} is specified manually using the procedure detailed in Section 2.1. The list $\mathbf{f}$ is hard-coded for each moon and calculated at run time from parameters in the SPICE planetary constants kernel and some manually determined excitation periods. An algorithmic method of determining the signal components, as is typical with the related method of Independent Components Analysis (Hyärinen & Oja, 2000; Hyvärinen, 2013), would have advantages and disadvantages. Removing the need for applying judgement or an arbitrary cutoff in acceptable residual power would improve the reproducibility of the determined excitation periods. However, drift in orbital and rotational parameters over time suggests that prioritizing expected oscillation periods may result in excitation moments that are of greater explanatory value in magnetic sounding investigations, and may be more accurate when extrapolated beyond the calculated time series era.

Calculation of spherical harmonics and their derivatives for intrinsic field models is limited in *PlanetMag* to degree 10. We have written bespoke functions for this purpose, which speeds up calculations dramatically because of the recursion relations used to evaluate arbitrary spherical harmonics, and the more complicated solutions that are required for their derivatives, both of which are required to calculate magnetic fields from multipole moments. We evaluated the harmonics and their derivatives with Mathematica for all spherical harmonic calculations implemented in *PlanetMag* and *MoonMag*. Transcribing these to machine-readable calculations and validating the result was a tedious process. Although future versions may include calculations to greater than degree 10, the induced fields at the locations of the large moons are primarily dominated by multipole moments of octupole order and below. Current sheet models typically have a large influence on the field experienced by each moon, and at their orbital distances typically the dipole moment is the only significant multipole moment. Therefore, we caution users of the software about its use in regions near the planet, where the unmodeled high-degree moments will have the greatest effect, and very far from the planet, where current sheet models are less accurate, but we consider the current implementation well-suited for application near the moons.

PlanetMag is the first open-source package to feature the calculation of the excitation moments $\mathbf{B}^e$ critical for magnetic sounding investigations. It is also the first software supporting the evaluation of magnetic field models across the outer solar system with SPICE integration, which extends its utility far beyond our intended development purpose, which is the precise calculation of $\mathbf{B}^e$. Complex excitation moments determined with as much attention to the well-known orbital and rotational parameters of the planets and moons as we have included enable time-dependent comparisons to spacecraft data of planetary and induced fields with unprecedented accuracy. We make this software and data available so that they may be used to improve current estimates and future analyses of spacecraft magnetic data.

Open Research

Data used in this work were generated using the open-source *PlanetMag* software hosted on GitHub (`https://github.com/coreyjcochrane/PlanetMag`). A Zenodo archive of the most recent version is available at `https://doi.org/10.5281/zenodo.10554762` (Styczinski & Cochrane, 2024a). *PlanetMag* is released under an Apache-2.0 license. The v1.0.2 release associated with this manuscript is archived at `https://doi.org/10.5281/zenodo.10864719` (Styczinski & Cochrane, 2024b). A Zenodo archive of the output data for excitation moments of the major moons with the default planetary field models (Tables 2 and 3) is available at `https://doi.org/10.5281/zenodo.10864716` (Styczinski & Cochrane, 2024c). This work uses products from the NASA Planetary Data System from several volumes: VG2-U-MAG-4-SUMM-U1COORDS-48SEC-V1.0 (Ness, 1993), VG2-N-MAG-4-SUMM-NLSCOORDS-12SEC-V1.0 (Ness, 1989), GO-J-MAG-3-RDR-MAGSPHERIC-SURVEY-V1.0 (Kivelson et al., 1997b), GO-J-MAG-3-RDR-HIGHRES-V1.0 (Kivelson et al., 1997a), CO-E/SW/J/S-MAG-4-SUMM-1MINAVG-V2.1 (Dougherty et al., 2019), and JNO-J-3-FGM-CAL-V1.0 (Connerney, 2022).

Acknowledgments

Portions of this work was carried out at the Jet Propulsion Laboratory, California Institute of Technology, under a contract with NASA (80NM0018D0004). The authors acknowledge that portions of this work have been carried out on the traditional lands of the Western Shoshone, Northern and Southern Paiute, Washoe, and Tongva peoples. M.J.S. was supported by an appointment to the NASA Postdoctoral Program at the Jet Propulsion Laboratory, California Institute of Technology, administered by Oak Ridge Associated Universities under a contract with NASA (80HQTR21CA005). M.J.S. thanks C. Baker for suggestions in setting up documentation for *PlanetMag*.

References

Acton, C. H. (1996). Ancillary data services of nasa's navigation and ancillary information facility. *Planetary and Space Science*, *44*(1), 65-70. (Planetary Data System) doi: 10.1016/0032-0633(95)00107-7

Arridge, C. S., & Eggington, J. W. B. (2021). Electromagnetic induction in the icy satellites of Uranus. *Icarus*, 114562. doi: 10.1016/j.icarus.2021.114562

Barik, A., & Angappan, R. (2024a). *AnkitBarik/planetMagFields: v1.4 : Support for multiple field models* [Software]. Zenodo. doi: 10.5281/zenodo.10685863

Barik, A., & Angappan, R. (2024b). *planetMagFields: A Python package for analyzing and plotting planetary magnetic field data.*

Biersteker, J. B., Weiss, B. P., Cochrane, C. J., Harris, C. D. K., Jia, X., Khurana, K. K., ... Raymond, C. A. (2023). Revealing the interior structure of icy moons with a Bayesian approach to magnetic induction measurements. *The Planetary Science Journal*, *4*(4), 62.

Blöcker, A., Saur, J., & Roth, L. (2016). Europa's plasma interaction with an inhomogeneous atmosphere: Development of Alfvén winglets within the Alfvén wings. *Journal of Geophysical Research: Space Physics*, *121*(10), 9794–9828.

Burton, M. E., Dougherty, M. K., & Russell, C. T. (2010). Saturn's internal planetary magnetic field. *Geophysical Research Letters*, *37*(24).

Cao, H., Dougherty, M. K., Hunt, G. J., Provan, G., Cowley, S. W. H., Bunce, E. J., ... Stevenson, D. J. (2020). The landscape of Saturn's internal magnetic field from the Cassini Grand Finale. *Icarus*, *344*, 113541.

Cochrane, C. J., Persinger, R. R., Vance, S. D., Midkiff, E. L., Castillo-Rogez, J., Luspay-Kuti, A., ... Prockter, L. M. (2022). Single-and multi-pass magnetometric subsurface ocean detection and characterization in icy worlds using Principal Component Analysis (PCA): Application to Triton. *Earth and Space Science*, *9*(2), e2021EA002034.

Cochrane, C. J., Vance, S. D., Nordheim, T. A., Styczinski, M. J., Masters, A., & Regoli, L. H. (2021). In search of subsurface oceans within the uranian moons. *Journal of Geophysical Research: Planets*, *126*(12), e2021JE006956.

Connerney, J. E. P. (1987). The magnetospheres of Jupiter, Saturn, and Uranus. *Reviews of Geophysics*, *25*(3), 615–638.

Connerney, J. E. P. (1992). Doing more with Jupiter's magnetic field. In

H. O. Rucker, S. J. Bauer, & M. L. Kaiser (Eds.), *Planetary radio emissions iii* (pp. 13–33). Austrian Academy of Sciences Press.

Connerney, J. E. P. (2007). Planetary magnetism. In T. Spohn (Ed.), *Treatise on geophysics* (Vol. 10). Elsevier. doi: 10.1016/B978-044452748-6.00159-0

Connerney, J. E. P. (2022). *Juno MAG CALIBRATED DATA J V1.0* (Vol. JNO-J-3-FGM-CAL-V1.0) [data]. NASA Planetary Data System. doi: 10.17189/1519711

Connerney, J. E. P., Acuña, M. H., & Ness, N. F. (1981). Modeling the jovian current sheet and inner magnetosphere. *Journal of Geophysical Research: Space Physics*, *86*(A10), 8370–8384.

Connerney, J. E. P., Acuña, M. H., & Ness, N. F. (1992). The magnetic field of Neptune. *Journal of Geophysical Research: Space Physics*, *96*(S01), 19023–19042. doi: 9610.1016/0273-1177(92)90394-D

Connerney, J. E. P., Acuña, M. H., Ness, N. F., & Satoh, T. (1998). New models of Jupiter's magnetic field constrained by the Io flux tube footprint. *Journal of Geophysical Research: Space Physics*, *103*(A6), 11929–11939.

Connerney, J. E. P., Kotsiaros, S., Oliversen, R. J., Espley, J. R., Joergensen, J. L., Joergensen, P. S., . . . Levin, S. M. (2018). A new model of Jupiter's magnetic field from Juno's first nine orbits. *Geophysical Research Letters*, *45*(6), 2590–2596.

Connerney, J. E. P., Timmins, S., Herceg, M., & Joergensen, J. L. (2020). A jovian magnetodisc model for the juno era. *Journal of Geophysical Research: Space Physics*, *125*(10). doi: 10.1029/2020ja028138

Connerney, J. E. P., Timmins, S., Oliversen, R. J., Espley, J. R., Joergensen, J. L., Kotsiaros, S., . . . Levin, S. M. (2022). A new model of jupiter's magnetic field at the completion of juno's prime mission. *Journal of Geophysical Research: Planets*, *127*(2). Retrieved from `https://doi.org/10.1029%2F2021je007055` doi: 10.1029/2021je007055

Dougherty, M. K., Cao, H., Khurana, K. K., Hunt, G. J., Provan, G., Kellock, S., . . . Southwood, D. J. (2018). Saturn's magnetic field revealed by the Cassini Grand Finale. *Science*, *362*(6410), eaat5434. doi: 10.1126/science.aat5434

Dougherty, M. K., Kellock, A. P., Slootweg, A. P., Achilleos, N., Joy, S. P., & Mafi, J. N. (2019). *CASSINI ORBITER MAG CALIBRATED SUMMARY AV-*

ERAGED V2.1 (Vol. CO-E/SW/J/S-MAG-4-SUMM-1MINAVG-V2.1) [data]. NASA Planetary Data System. doi: 10.17189/5rhj-sm88

Fletcher, L. N., Cavalié, T., Grassi, D., Hueso, R., Lara, L. M., Kaspi, Y., ... Costa, M. (2023). Jupiter science enabled by ESA's Jupiter Icy Moons Explorer. *Space Science Reviews*, *219*(7), 53. doi: 10.1007/s11214-023-00996-6

Gorski, K. M., Hivon, E., Banday, A. J., Wandelt, B. D., Hansen, F. K., Reinecke, M., & Bartelmann, M. (2005). HEALPix: A framework for high-resolution discretization and fast analysis of data distributed on the sphere. *The Astrophysical Journal*, *622*(2), 759.

Hand, K. P., & Chyba, C. F. (2007). Empirical constraints on the salinity of the europan ocean and implications for a thin ice shell. *Icarus*, *189*(2), 424–438. doi: 10.1016/j.icarus.2007.02.002

Harris, C. D. K., Jia, X., Slavin, J. A., Toth, G., Huang, Z., & Rubin, M. (2021). Multi-fluid MHD simulations of Europa's plasma interaction under different magnetospheric conditions. *Journal of Geophysical Research: Space Physics*, *126*(5), e2020JA028888. doi: 10.1029/2020JA028888

Herbert, F. (2009). Aurora and magnetic field of Uranus. *Journal of Geophysical Research: Space Physics*, *114*(A11).

Hyärinen, A., & Oja, E. (2000). Independent component analysis: algorithms and applications. *Neural Networks*, *13*(4), 411–430. doi: 10.1016/S0893-6080(00)00026-5

Hyvärinen, A. (2013). Independent component analysis: recent advances. *Philosophical Transactions of the Royal Society A: Mathematical, Physical and Engineering Sciences*, *371*(1984), 20110534.

Jackson, J. D. (1999). *Classical electrodynamics.* John Wiley & Sons. doi: 10.1119/1.19136

James, M. K., Provan, G., Kamran, A., Wilson, R. J., Vogt, M. F., Brennan, M. J., & Cowley, S. W. H. (2024a). *JupiterMag* [Software]. Zenodo. doi: 10.5281/zenodo.6822191

James, M. K., Provan, G., Kamran, A., Wilson, R. J., Vogt, M. F., Brennan, M. J., & Cowley, S. W. H. (2024b). *libjupitermag* [Software]. Zenodo. doi: 10.5281/zenodo.7306035

Khurana, K. K. (1997). Euler potential models of Jupiter's magnetospheric field.

Journal of Geophysical Research: Space Physics, *102*(A6), 11295–11306.

Khurana, K. K. (2020). *KMAG - kronian magnetic field model* [Software]. Zenodo. doi: 10.5281/zenodo.4080293

Khurana, K. K., Jia, X., Kivelson, M. G., Nimmo, F., Schubert, G., & Russell, C. T. (2011). Evidence of a global magma ocean in Io's interior. *Science*, *332*(6034), 1186–1189.

Khurana, K. K., & Schwarzl, H. K. (2005). Global structure of Jupiter's magnetospheric current sheet. *Journal of Geophysical Research: Space Physics*, *110*(A7).

Kivelson, M. G., Khurana, K. K., Russell, C. T., Volwerk, M., Walker, R. J., & Zimmer, C. (2000). Galileo magnetometer measurements: A stronger case for a subsurface ocean at Europa. *Science*, *289*(5483), 1340–1343. doi: 10.1126/science.289.5483.1340

Kivelson, M. G., Khurana, K. K., Russell, C. T., Walker, R. J., Joy, S. P., & Mafi, J. N. (1997a). *GALILEO ORBITER AT JUPITER CALIBRATED MAG HIGH RES V1.0* (Vol. GO-J-MAG-3-RDR-HIGHRES-V1.0) [data]. NASA Planetary Data System. doi: 10.17189/1519667

Kivelson, M. G., Khurana, K. K., Russell, C. T., Walker, R. J., Joy, S. P., & Mafi, J. N. (1997b). *JUPITER MAG MAGNETOSPHERIC SURVEY V1.0* (Vol. GO-J-MAG-3-RDR-MAGSPHERIC-SURVEY-V1.0) [data]. NASA Planetary Data System. doi: 10.17189/1519668

Kivelson, M. G., Khurana, K. K., Stevenson, D. J., Bennett, L., Joy, S., Russell, C. T., ... Polanskey, C. (1999). Europa and Callisto: Induced or intrinsic fields in a periodically varying plasma environment. *Journal of Geophysical Research: Space Physics*, *104*(A3), 4609–4625.

Kivelson, M. G., Khurana, K. K., & Volwerk, M. (2002). The permanent and inductive magnetic moments of Ganymede. *Icarus*, *157*(2), 507–522.

Markovsky, I., & Van Huffel, S. (2007). Overview of total least-squares methods. *Signal Processing*, *87*(10), 2283–2302. (Special Section: Total Least Squares and Errors-in-Variables Modeling) doi: 10.1016/j.sigpro.2007.04.004

Ness, N. F. (1989). *VG2 NEP MAG RESAMPLED SUMMARY NLS COORDINATES 12SEC V1.0* (Vol. VG2-N-MAG-4-SUMM-NLSCOORDS-12SEC-V1.0) [data]. NASA Planetary Data System. doi: 10.17189/1519975

Ness, N. F. (1993). *VG2 URA MAG RESAMPLED SUMMARY U1 COORDINATES 48SEC V1.0* (Vol. VG2-U-MAG-4-SUMM-U1COORDS-48SEC-V1.0) [data]. NASA Planetary Data System. doi: 10.17189/1520034

Plattner, A. M., Johnson, C. L., Styczinski, M. J., Vance, S. D., & Mills, A. C. (2023). On Ganymede's magnetic quadrupolar strength. *Planetary Science Journal*, *4*(134). doi: 10.3847/PSJ/acde7f

Rusaitis, L. (2022). *Python package for KMAG field model* [Software]. Zenodo. doi: 10.5281/zenodo.6793395

Schilling, N., Neubauer, F. M., & Saur, J. (2007). Time-varying interaction of Europa with the jovian magnetosphere: Constraints on the conductivity of Europa's subsurface ocean. *Icarus*, *192*(1), 41–55. doi: 10.1016/j.icarus.2007.06.024

Schilling, N., Neubauer, F. M., & Saur, J. (2008). Influence of the internally induced magnetic field on the plasma interaction of Europa. *Journal of Geophysical Research: Space Physics*, *113*(A3).

Schubert, G., & Soderlund, K. M. (2011). Planetary magnetic fields: Observations and models. *Physics of the Earth and Planetary Interiors*, *187*(3-4), 92–108.

Seufert, M., Saur, J., & Neubauer, F. M. (2011). Multi-frequency electromagnetic sounding of the Galilean moons. *Icarus*, *214*(2), 477–494. doi: 10.1016/j.icarus.2011.03.017

Stanley, S., & Glatzmaier, G. A. (2010). Dynamo models for planets other than Earth. *Space science reviews*, *152*(1-4), 617–649.

Styczinski, M. J. (2023). *itsmoosh/MoonMag* [Software]. Zenodo. Retrieved from `https://doi.org/10.5281/zenodo.5002955` doi: 10.5281/zenodo.5002955

Styczinski, M. J., & Cochrane, C. J. (2024a). *coreyjcochrane/PlanetMag* [Software]. Zenodo. doi: 10.5281/zenodo.10554762

Styczinski, M. J., & Cochrane, C. J. (2024b). *coreyjcochrane/PlanetMag: Model updates following publication peer review* [Software]. Zenodo. doi: 10.5281/zenodo.10864719

Styczinski, M. J., & Cochrane, C. J. (2024c). *Magnetic excitation moments for large moons of the giant planets* [Dataset]. Zenodo. doi: 10.5281/zenodo.10864716

Styczinski, M. J., Cochrane, C. J., & Vance, S. D. (2021). *Degree-1 magnetic excitation spectra for large moons in the outer solar system* [Dataset]. Zenodo. doi:

10.5281/zenodo.5057572

Styczinski, M. J., Vance, S. D., Harnett, E. M., & Cochrane, C. J. (2022). A perturbation method for evaluating the magnetic field induced from an arbitrary, asymmetric ocean world analytically. *Icarus*, *376*(1), 114840. doi: 10.1016/j.icarus.2021.114840

Vance, S. D., Craft, K. L., Shock, E., Schmidt, B. E., Lunine, J. I., Hand, K. P., ... Elder, C. M. (2023). Investigating Europa's habitability with Europa Clipper. *Space Science Reviews*, *219*(81). doi: 10.1007/s11214-023-01025-2

Vance, S. D., Styczinski, M. J., Bills, B. G., Cochrane, C. J., Soderlund, K. M., Gómez-Pérez, N., & Paty, C. (2021). Magnetic induction responses of Jupiter's ocean moons including effects from adiabatic convection. *Journal of Geophysical Research: Planets*, *126*(2), e2020JE006418. doi: 10.1029/2020JE006418

Weiss, B. P., Biersteker, J. B., Colicci, V., Goode, A., Castillo-Rogez, J. C., Petropoulos, A. E., & Balint, T. S. (2021). Searching for subsurface oceans on the moons of Uranus using magnetic induction. *Geophysical Research Letters*, *48*(19), e2021GL094758.

Wilson, R. J., Vogt, M. F., Provan, G., Kamran, A., James, M. K., Brennan, M. J., & Cowley, S. W. H. (2022). *Psh: Planetary Spherical Harmonics community code* [Software]. Zenodo. doi: 10.5281/zenodo.7327992

Wilson, R. J., Vogt, M. F., Provan, G., Kamran, A., James, M. K., Brennan, M. J., & Cowley, S. W. H. (2023). Internal and external Jovian magnetic fields: Community code to serve the magnetospheres of the outer planets community. *Space Science Reviews*, *219*(1), 15. doi: 10.1007/s11214-023-00961-3

Zimmer, C., Khurana, K. K., & Kivelson, M. G. (2000). Subsurface oceans on Europa and Callisto: Constraints from Galileo magnetometer observations. *Icarus*, *147*(2), 329–347. doi: 10.1006/icar.2000.6456

Supporting information for "*PlanetMag:* Software for evaluation of outer planet magnetic fields and corresponding excitations at their moons"

M. J. Styczinski[1] and C. J. Cochrane[2]

[1]Blue Marble Space Institute of Science, Seattle, Washington, USA

[2]Jet Propulsion Laboratory, California Institute of Technology, Pasadena, California, USA

Contents of this file

1. Text S1
2. Figures S1–S2

Introduction

This supplement contains a detailed description of the frames implemented in *PlanetMag* and definitions of their associated coordinate systems.

S1. Frames and coordinate systems

Below, we describe the IAU frames and those considered in past work for comparison. All frames described here are implemented in *PlanetMag* via a custom frames kernel for use with SPICE. Past studies have typically used $\phi\Omega$ coordinate systems (e.g., Zimmer et al., 2000) or spherical coordinates in the System III frame (SPRH) of the parent planet (Seufert et al., 2011; Arridge & Eggington, 2021) for evaluating the excitation moments. Although $\phi\Omega$ and SPRH coordinate systems are preferable for modeling and analysis of magnetospheric plasmas, neither is fixed to the surface of the moon. Because all large moons in our solar system rotate synchronously, the IAU axes can be approximated by one or more 90° rotations from SPRH or $\phi\Omega$ coordinates. However, the exact rotations vary throughout the orbital and true anomaly periods by up to several degrees, which introduces artifacts to the excitation spectrum.

In every case where a direction is specified from one body to another, or reference is made to a body's center, the center of mass is implied for each.

S1.1. IAU, System III, and SPRH frames

Parameterizations for IAU frames are adopted by resolution at an IAU General Assembly and described in reports of the IAU Working Group on Cartographic Coordinates and Rotational Elements, which we call the CCWG. IAU frames are defined for all major planetary objects in the solar system and are body-fixed and planetocentric, with the origin at the body center. In these frames, which are built-in to SPICE, the $\hat{z}$ axis is always directed along the rotation axis of the body, on the north side of the invariable plane—defined by the net angular momentum vector of the entire solar system. The northward normal of the invariable plane defines the $\hat{z}$ direction for International Celestial Reference System (ICRF), an inertial frame used in evaluating planetary ephemerides (the ICRF $\hat{x}$ direction is through the Earth equator at the vernal equinox at J2000).

For all planets and large moons except those in the Uranus system and Triton (which orbits Neptune in a retrograde direction), the IAU $\hat{z}$ axis is directed along the angular momentum vector of the body relative to its parent. For the Uranus system and Triton, $\hat{z}$ is in the opposite direction. The $\hat{x}$ direction is orthogonal to $\hat{z}$, directed from the body center toward the plane containing an arbitrary feature used to define the 0° (prime meridian) longitude for the body. For all moons, this is a feature intended to direct $\hat{x}$ approximately toward the parent planet. For all planets, this is a feature intended to face a particular direction at a particular epoch (Section S1.1.1). The $\hat{y}$ direction completes a right-handed coordinate system, approximately along the orbital velocity vector relative to the parent planet for the uranian moons and Triton and opposite the orbital velocity vector for all other large moons. The IAU x axis tracks the 0° longitude feature, and so moves with the surface of the body.

For the giant planets, which generally lack stable surface features, the IAU frame typically rotates at the same rate as the System III frame (Archinal et al., 2018a), which is defined by periodicity in the magnetic field of the planet or features tied to the magnetic field. These features are believed to be fixed to the motion of the deep interior of the planet. The System III frame always has the $\hat{z}$ direction along the angular momentum vector of the planet and 0° longitude along the direction of the IAU prime meridian. SPRH, a coordinate system sometimes used in spacecraft data analysis, is a spherical representation of the System III frame.

For Jupiter and Saturn, the IAU and System III frames are identical. For Uranus, the IAU frame has $\hat{y}$ and $\hat{z}$ reversed from the System III frame. For Neptune, the IAU frame was changed in the 2015 CCWG Report (Archinal et al., 2018b) to be a System II frame, which rotates along with stable atmospheric features. This definition has not yet been implemented in SPICE as of planetary constants kernel (PCK) `pck00010.tpc` and the IAU frame is not used for Neptune in *PlanetMag*. The latest PCK available, `pck00011.tpc`, implements this System II frame for Neptune, which differs from that used to derive the available magnetic field models for Neptune. We continue to use `pck00010.tpc` in *PlanetMag* for this reason. A more detailed description of the definitions of the IAU frames for the giant planets follows.

S1.1.1. IAU frame definitions for the giant planets

Jupiter — System III (1965): This frame is described well by P. Seidelmann and Divine (1977), and was adopted by the CCWG by the time of their first report (Davies et al., 1980). The rotation rate was selected based on many years of radio observations. It was revised in the 2000 report (P. K. Seidelmann et al., 2002) to be more precise based on recent work, but reverted in the 2009 report (Archinal et al., 2011) due to subsequent challenges raised against the updated rotation rate. The prime meridian is defined such that System III (1957.0) longitudes, which used a slightly different rotation period, coincide with System II longitudes at the 1957.0 epoch. However, a mistake in evaluating System II at 1957-01-01 00:00:00.000 UTC instead of the same time TDB (Coordinated Universal Time vs. Barycentric Dynamical Time, a difference of about 41.2 s) in calculating the observed central meridian longitude means the agreement is only approximate. Jupiter System II revolves with the mid-latitude atmospheric rotation rate (Dessler, 2002). Ultimately, the System III prime meridian is arbitrary and since the frame has seen widespread adoption in magnetic modeling, it is sufficient to use the J2000 definition as a reference.

Saturn — System III: This frame was defined by Desch and Kaiser (1981) as the Saturn Longitude System (SLS) and was adopted by the CCWG in the 1982 report (Davies et al., 1983), with the planetary rotation period revised in a private communication from M. L. Kaiser to M. E. Davies. Also referred to as L1 in Voyager 1/2 data hosted on the Planetary Data System (PDS). The prime meridian is selected to coincide with the Saturn ascending node of the planet's orbit on its equator at the 1980.0 epoch, 1980-01-01 00:00:00.000 UTC. The 1982 report (Davies et al., 1983) contains expressions for the prime meridian location relative to the J2000 epoch, which remain unchanged in the latest CCWG report (Archinal et al., 2018a). Axisymmetry of the Saturn magnetic moments (no moments are even reported for $m \neq 0$ in the literature) mean that the prime meridian definition does not impact modeling of the internal field, but the same is not true of the external current systems (Andrews et al., 2019). Subsequent research has resulted in alternative systems, namely SLS2 (Kurth et al., 2007) and SLS3 (Kurth et al., 2008). These systems vary the rotation rate to maintain an observed peak in radio intensities at 100° subsolar longitude. The varying rotation rate implies that these coordinate systems may not rotate with the deep interior of the planet, and the SLS system remains that preferred by the CCWG.

Uranus — System III: The first CCWG report defined the prime meridians of Saturn, Uranus, and Neptune to coincide with the ICRF x axis (direction of Earth vernal equinox from the solar system barycenter) at the J1950 epoch, 1950-01-01 00:00:00 TDB. Uranus is the only planet that still retains this definition in the latest report (Archinal et al., 2018a). The rotation rate was updated in the 1985 report (Davies et al., 1986) based on preliminary analysis from Voyager 2, with the prime meridian being briefly (and perhaps accidentally) set to the ICRF x direction at J2000 for this report only. The rotation rate, based on Desch, Connerney, and Kaiser (1986), has not been updated since the 1986 report. The z axis for the IAU frame is opposite to the rotation direction, because the angular momentum vector is greater than 90° away from the z axis of the ICRF frame, and IAU convention stipulates this condition. This frame is not typically used in analysis of magnetic data, primarily because of the ubiquity of spherical coordinates with the polar axis aligned to the angular momentum vector, in opposition to the IAU definition.

Neptune — System II: Following the Voyager 2 flyby of Neptune, a radio-derived rotation period based on Warwick et al. (1989) was adopted by the IAU. The 1950.0 ICRF x axis definition for the prime meridian was retained until the current System II definition was adopted in the 2015 report (Archinal et al., 2018b) based on observations of remarkably stable cloud features reported by Karkoschka (2011). The System II definition uses the rotation period inferred from the South Polar Feature and South Polar Wave identified by Karkoschka (2011), and the prime meridian is located at the average of the longitudes of both features. This meridian is stated to coincide with the System III (1950.0) meridian at 1989-08-03 12:00:00 UTC. The System II frame is not yet implemented in the latest recommended version of the SPICE planetary constants kernel, `pck00010.tpc`.

S1.2. Frames for planetary field models

Each intrinsic field model implemented in *PlanetMag* is evaluated using the coordinates specified in the peer-reviewed publication that describes the model. Generally, these coordinates match those in which the available spacecraft measurements are reported for the planet. Current sheet models often use unique coordinate systems, but these are referenced to the same standard systems. All models for a particular planet use a single coordinate system, as follows.

Jupiter: System III (1965), implemented as the `IAU_JUPITER` frame in SPICE.

Saturn: Saturn Longitude System (SLS), also known as S1, implemented as the `IAU_SATURN` frame in SPICE.

Uranus: Uranus Longitude System (ULS), also known as U1, as defined by Ness et al. (1986) and named by Herbert (2009). $\hat{z}$ is aligned with the planet's angular momentum vector, the prime meridian is arbitrarily defined using the Voyager 2 trajectory, and the frame rotates along with the intrinsic magnetic moments. This frame is obtained by inverting the z axis of the `IAU_URANUS` frame and rotating to set the Voyager 2 position at 1986-01-24 18:00:00, about 1 s from closest approach (CA), to be 302°W in the ULS frame. From the most up-to-date SPICE kernel reconstructing the Voyager 2 trajectory, `vgr2.ura111.bsp`, and the `pck00010.tpc` planetary constants kernel, the IAU longitude of the spacecraft at this time was about 225.3°E. The ULS frame is a constant offset from the IAU frame and thus rotates with the IAU frame. The Voyager 2 magnetic measurements and trajectory from the Uranus flyby are reported in ULS coordinates.

Neptune: Neptune Longitude System (NLS), as defined by Connerney, Acuña, and Ness (1992). $\hat{z}$ is aligned with the planet's angular momentum vector, defined by Connerney et al. (1992) to have right ascension $\alpha_0 = 298.90°$ and declination $\delta_0 = 42.84°$, which we assume to be in reference to the ICRF frame at J2000. The prime meridian orientation is defined using 167.7°W at 0356 spacecraft event time (SCET, equivalent to UTC in this case) on day-of-year 237 (August 25) of the year 1989. The Voyager 2 trajectory determined from the latest SPICE kernels (`vg2_nep097.bsp`) in this frame does not match the data reported in PDS (volume VG2-N-MAG-4-SUMM-NLSCOORDS-12SEC-V1.0). We have implemented the frame defined by Connerney et al. (1992) as `NLS_RADEC` and a second frame, `NLS`, that is equivalent to the `IAU_NEPTUNE` frame implemented in SPICE based on the 2009 CCWG report (Archinal et al., 2011) but rotated to place Voyager 2 at a planetocentric west longitude of 167.7°, a rotation of 12.0140°. The `NLS` frame much more closely approximates the Voyager 2 trajectory detailed in this frame along with the magnetic data on PDS, but some systematic offset is still present from an unknown source. See Figure S1 for a comparison of the NLS trajectory against that reported in the PDS data.

S1.3. Frames for magnetic investigation of moons

Past investigations have primarily used $\phi\Omega$ frames. These frames are common in analysis of plasma flow and moon–plasma interactions because the axes rotate along with the moon as it orbits and the xy plane is coplanar with that of the planet's System III frame, related by a rotation about $\hat{z}$. In $\phi\Omega$ frames, the $\hat{z}$ direction is aligned to the parent planet's spin angular momentum vector, $\hat{x} = -\hat{r} \times \hat{z}$, where $\hat{r}$ is the direction from the parent planet to the moon, and $\hat{y}$ completes the right-handed set. $\hat{y}$ is approximately toward the parent planet, $\hat{x}$ is in the corotation direction—approximately along the orbital velocity vector, and $\hat{z}$ is approximately along the moon's angular momentum vector in the case of natural moons that orbit near the planet's spin equator. Because each moon's orbit is elliptical, the axes rotate in a non-uniform fashion, faster near periapsis and slower near apoapsis. A comparison between the IAU frame, which is fixed to the body surface, and the $\phi\Omega$ frame for Europa, E$\phi\Omega$, is shown in Figure S2. In *PlanetMag*, we have implemented $\phi\Omega$ frames only for the moons of Jupiter, to facilitate comparison to past studies. These frames are available in *PlanetMag* as `IO_PHI_O`, `EUROPA_PHI_O`, etc. Note also that the above descriptions of these frames may vary for retrograde orbits, as in the case of Triton.

S1.4. Additional frames for evaluation of models in the literature

For convenience and comparison to prior work, we have also implemented the following frames, all of which are centered on the planet:

Planet–Sun–Orbit: $\hat{x}$ is directed toward the Sun. $\hat{y}$ is directed along the component of the Sun's instantaneous inertial velocity vector, as seen from the planet, that is normal to $\hat{x}$, and $\hat{z}$ completes the right-handed set. Available in *PlanetMag* as `JSO`, `KSO`, `USO`, and `NSO` for Jupiter, Saturn, Uranus, and Neptune, respectively.

Planet–Sun–Magnetic: $\hat{x}$ is directed toward the Sun. $\hat{y}$ is along $\hat{\mathbf{M}} \times \hat{x}$, where $\mathbf{M}$ is the instantaneous magnetic dipole moment vector. $\hat{z}$ completes the right-handed set. A model must be selected for the orientation of the dipole moment. These frames are available in *PlanetMag* with the following model dipole orientations: `JSM` — O4 (Acuña & Ness, 1976), used in magnetosphere shape calculations in KS2005 model (Khurana & Schwarzl, 2005); `KSM` — Cassini 11 (Dougherty et al., 2018); `USM` — Offset, tilted dipole (OTD) (Ness et al., 1986), used in magnetopause field calculations of Arridge and Eggington (2021); `NSM` — O8 (Connerney et al., 1992). Originally defined by Acuña and Ness (1976) and given this name in Bagenal and Wilson (2016, `https://lasp.colorado.edu/home/mop/files/2015/02/CoOrd_systems12.pdf`).

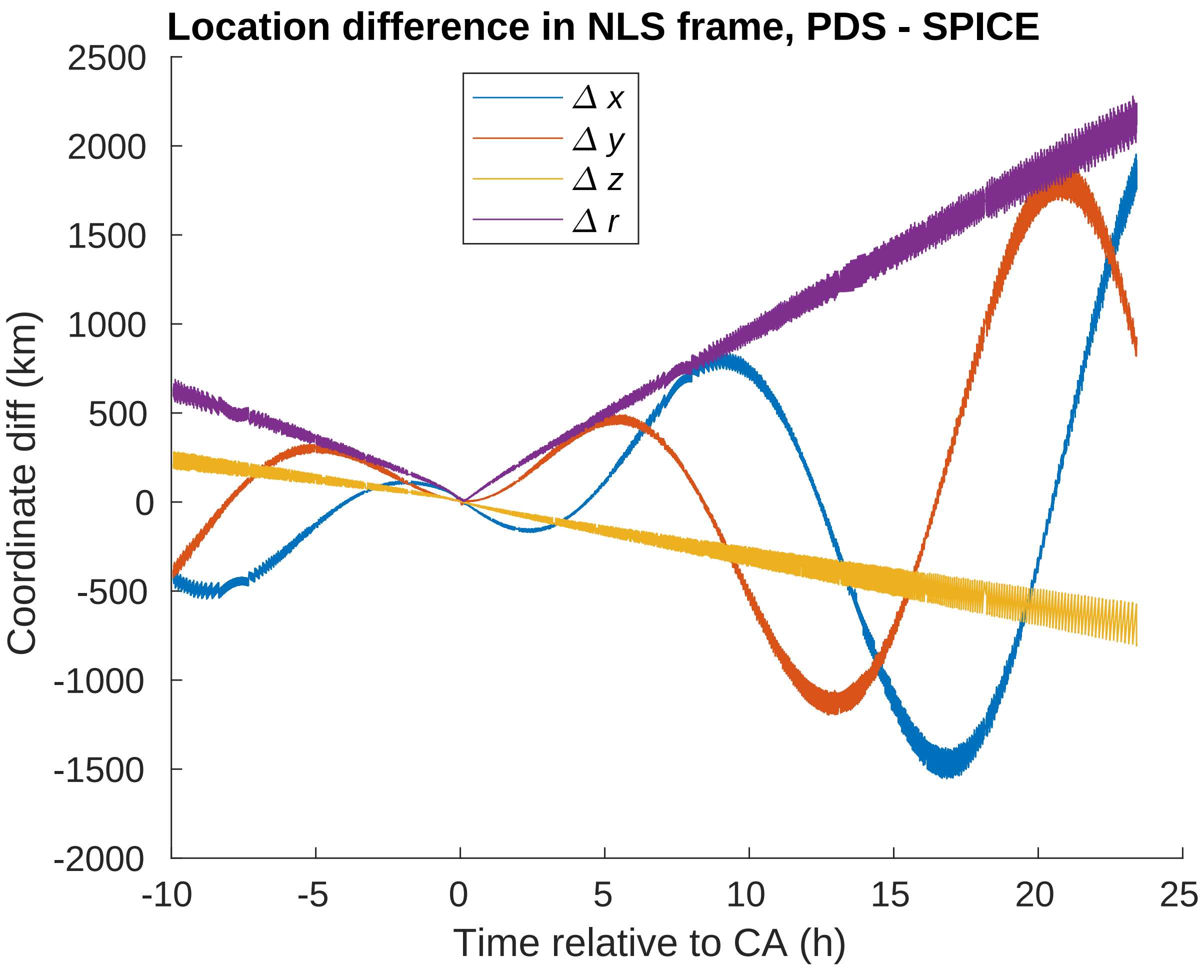

Figure S1. Comparison of the Voyager 2 trajectory in the NLS frame as reported in PDS data (volume VG2-N-MAG-4-SUMM-NLSCOORDS-12SEC-V1.0) vs. our implementation of the frame using the latest reconstruction using SPICE kernels.

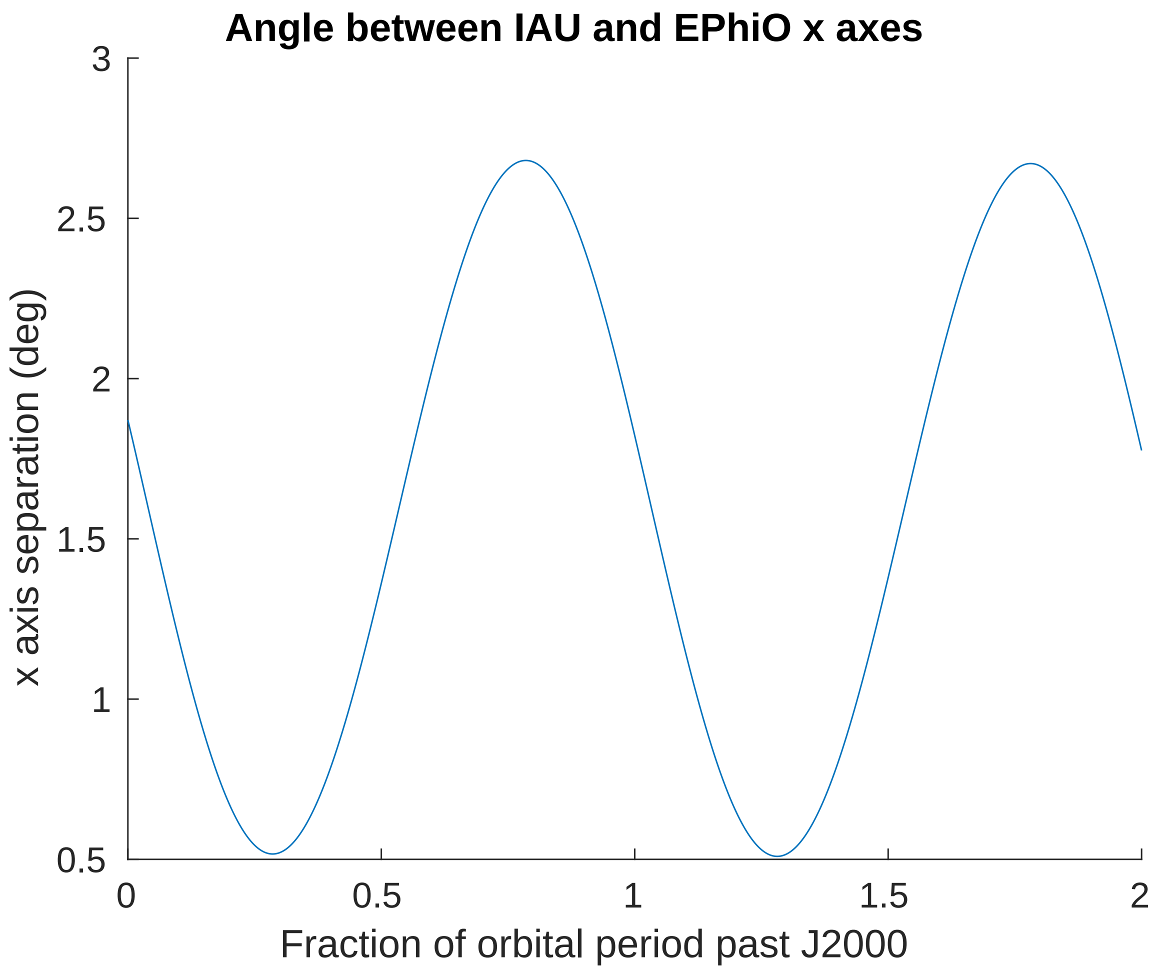

Figure S2. Angle between $\hat{x}$ for the IAU frame for Europa and the $\mathrm{E}\phi\Omega$ coordinate system commonly used in past magnetic sounding investigations throughout the first 2 orbital periods following the J2000 epoch. The IAU frame is fixed to the body surface; the $\mathrm{E}\phi\Omega$ axes vary throughout Europa's orbital period as it librates.

Planet–Dipole–Solar–Zenith: $\hat{z}$ is directed toward the Sun. $\hat{y}$ is along $\hat{\mathbf{M}} \times \hat{z}$, where $\hat{\mathbf{M}}$ is along the dipole moment vector and the same models are selected as in the Planet–Sun–Magnetic frames. $\hat{x}$ completes the right-handed set, approximately antiparallel to $\hat{\mathbf{M}}$. Available in *PlanetMag* as `JDSZ`, `KDSZ`, `UDSZ`, and `NDSZ`. This frame is described in application to Jupiter by Alexeev and Belenkaya (2005), but not named therein. Used in Arridge and Eggington (2021) magnetopause model based on shape defined by Shue et al. (1997), for which this frame makes evaluation simple.

Solar–Magnetic–Planet: $\hat{z}$ is along $\hat{\mathbf{M}}$ as defined in the models selected for the Planet–Sun–Magnetic frames. $\hat{y}$ is along $\hat{r}_{\mathrm{Sun}} \times \hat{z}$, where $\hat{r}_{\mathrm{Sun}}$ is directed toward the Sun. $\hat{x}$ completes the right-handed set. The xy plane of this frame is the magnetic dipole equator, and $\phi = 0$ in spherical coordinates in this frame coincides with the sub-solar longitude. Available in *PlanetMag* as `SMJ`, `SMK`, `SMU`, and `SMN`.

References

Acuña, M. H., & Ness, N. F. (1976). The main magnetic field of Jupiter. *Journal of Geophysical Research*, *81*(16), 2917–2922. doi: 10.1029/JA081i016p02917

Alexeev, I. I., & Belenkaya, E. S. (2005). Modeling of the Jovian magnetosphere. In *Annales geophysicae* (Vol. 23, pp. 809–826).

Andrews, D. J., Cowley, S. W. H., Provan, G., Hunt, G. J., Hadid, L. Z., Morooka, M. W., & Wahlund, J.-E. (2019). The structure of planetary period oscillations in saturn's equatorial magnetosphere: Results from the cassini mission. *Journal of Geophysical Research: Space Physics*, *124*(11), 8361–8395.

Archinal, B. A., Acton, C. H., A'Hearn, M. F., Conrad, A., Consolmagno, G. J., Duxbury, T., … Williams, I. P. (2018a). Report of the IAU working group on cartographic coordinates and rotational elements: 2015. *Celestial Mechanics and Dynamical Astronomy*, *130*(3), 22. doi: 10.1007/s10569-017-9805-5

Archinal, B. A., Acton, C. H., A'Hearn, M. F., Conrad, A., Consolmagno, G. J., Duxbury, T., … Williams, I. P. (2018b). Report of the IAU working group on cartographic coordinates and rotational elements: 2015. *Celestial Mechanics and Dynamical Astronomy*, *130*(3), 22. doi: 10.1007/s10569-017-9805-5

Archinal, B. A., A'Hearn, M. F., Bowell, E., Conrad, A., Consolmagno, G. J., Courtin, R., … others (2011). Report of the IAU working group on cartographic coordinates and rotational elements: 2009. *Celestial Mechanics and Dynamical Astronomy*, *109*(2), 101–135.

Arridge, C. S., & Eggington, J. W. B. (2021). Electromagnetic induction in the icy satellites of Uranus. *Icarus*, 114562. doi: 10.1016/j.icarus.2021.114562

Connerney, J. E. P., Acuña, M. H., & Ness, N. F. (1992). The magnetic field of Neptune. *Journal of Geophysical Research: Space Physics*, *96*(S01), 19023–19042. doi: 9610.1016/0273-1177(92)90394-D

Davies, M. E., Abalakin, V. K., Bursa, M., Lederle, T., Lieske, J. H., Rapp, R. H., … Tjuflin, Y. S. (1986). Report of the IAU/IAG/COSPAR working group on cartographic coordinates and rotational elements of the planets and satellites-1985. *Celestial mechanics*, *39*, 103–113.

Davies, M. E., Abalakin, V. K., Cross, C. A., Duncombe, R. L., Masursky, H., Morando, B., … Tjuflin, Y. S. (1980). Report of the IAU working group on cartographic coordinates and rotational elements of the planets and satellites. *Celestial mechanics*, *22*(3), 205–230.

Davies, M. E., Abalakin, V. K., Lieske, J. H., Seidelmann, P. K., Sinclair, A. T., Sinzi, A. M., … Tjuflin, Y. S. (1983). Report of the IAU working group on cartographic coordinates and rotational elements of the planets and satellites: 1982. *Celestial mechanics*, *29*(4), 309–321.

Desch, M. D., Connerney, J. E. P., & Kaiser, M. L. (1986). The rotation period of Uranus. *Nature*, *322*(6074), 42–43.

Desch, M. D., & Kaiser, M. L. (1981). Voyager measurement of the rotation period of Saturn's magnetic field. *Geophysical Research Letters*, *8*(3), 253–256.

Dessler, A. J. (2002). *Physics of the Jovian magnetosphere* (Vol. 3). Cambridge University Press.

Dougherty, M. K., Cao, H., Khurana, K. K., Hunt, G. J., Provan, G., Kellock, S., … Southwood, D. J. (2018). Saturn's magnetic field revealed by the Cassini Grand Finale. *Science*, *362*(6410), eaat5434. doi: 10.1126/science.aat5434

Herbert, F. (2009). Aurora and magnetic field of Uranus. *Journal of Geophysical Research: Space Physics*, *114*(A11).

Karkoschka, E. (2011). Neptune's rotational period suggested by the extraordinary stability of two features. *Icarus*, *215*(1), 439–448.

Khurana, K. K., & Schwarzl, H. K. (2005). Global structure of Jupiter's magnetospheric current sheet. *Journal of Geophysical Research: Space Physics*, *110*(A7).

Kurth, W. S., Averkamp, T. F., Gurnett, D. A., Groene, J. B., & Lecacheux, A. (2008). An update to a Saturnian longitude system based on kilometric radio emissions. *Journal of Geophysical Research: Space

Physics, *113*(A5).

Kurth, W. S., Lecacheux, A., Averkamp, T. F., Groene, J. B., & Gurnett, D. A. (2007). A Saturnian longitude system based on a variable kilometric radiation period. *Geophysical Research Letters*, *34*(2).

Ness, N. F., Acuña, M. H., Behannon, K. W., Burlaga, L. F., Connerney, J. E. P., Lepping, R. P., & Neubauer, F. M. (1986). Magnetic fields at Uranus. *Science*, *233*(4759), 85–89. doi: 10.1126/science.233.4759.85

Seidelmann, P., & Divine, N. (1977). Evaluation of Jupiter longitudes in System III (1965). *Geophysical Research Letters*, *4*(2), 65–68.

Seidelmann, P. K., Abalakin, V. K., Bursa, M., Davies, M. E., de Bergh, C., Lieske, J. H., ... Thomas, P. C. (2002). Report of the IAU/IAG working group on cartographic coordinates and rotational elements of the planets and satellites: 2000. *Celestial Mechanics and Dynamical Astronomy*, *82*(1), 83–111.

Seufert, M., Saur, J., & Neubauer, F. M. (2011). Multi-frequency electromagnetic sounding of the Galilean moons. *Icarus*, *214*(2), 477–494. doi: 10.1016/j.icarus.2011.03.017

Shue, J.-H., Chao, J. K., Fu, H. C., Russell, C. T., Song, P., Khurana, K. K., & Singer, H. J. (1997). A new functional form to study the solar wind control of the magnetopause size and shape. *Journal of Geophysical Research: Space Physics*, *102*(A5), 9497–9511. doi: 10.1029/97JA00196

Warwick, J. W., Evans, D. R., Peltzer, G. R., Peltzer, R. G., Romig, J. H., Sawyer, C. B., ... Zarka, P. (1989). Voyager planetary radio astronomy at Neptune. *Science*, *246*(4936), 1498–1501.

Zimmer, C., Khurana, K. K., & Kivelson, M. G. (2000). Subsurface oceans on Europa and Callisto: Constraints from Galileo magnetometer observations. *Icarus*, *147*(2), 329–347. doi: 10.1006/icar.2000.6456